Supplementary Information Appendix

Long-term stability in the circumpolar foraging range of a Southern Ocean predator between the eras of whaling and rapid climate change

Solène Derville*[1,2], Leigh G. Torres[1], Seth D. Newsome[3], Christopher J. Somes[4], Luciano O. Valenzuela[5,6,7], Hannah B. Vander Zanden[8], C. Scott Baker[1,9], Martine Bérubé[10,11], Geraldine Busquets-Vass[3,12], Kris Carlyon[13], Simon J. Childerhouse[14], Rochelle Constantine[15], Glenn Dunshea[16,17], Paulo A. C. Flores[18], Simon D. Goldsworthy[19,20], Brittany Graham[14], Karina Groch[21], Darren R. Gröcke[22], Robert Harcourt[23], Mark A. Hindell[24], Pavel Hulva[25,26], Jennifer A. Jackson[27], Amy S. Kennedy[28], David Lundquist[29], Alice. I. Mackay[19], Petra Neveceralova[25,30,31], Larissa Oliveira[32,33], Paulo H. Ott[32,34], Per J. Palsbøll[10,11], Nathalie J. Patenaude[35], Victoria Rowntree[7,36,6], Mariano Sironi[6,37], Els Vermeuelen[38], Mandy Watson[39], Alexandre N. Zerbini[28,40], Emma L. Carroll*[15]

1. Marine Mammal Institute, Oregon State University, Newport, Oregon, United States
2. UMR Entropie, French Institute of Research for Sustainable Development, Nouméa, New Caledonia
3. Biology Department, University of New Mexico, Albuquerque, New Mexico, United States
4. GEOMAR Helmholtz Centre for Ocean Research Kiel, Kiel, Germany
5. Consejo Nacional de Investigaciones Científicas y Técnicas (CONICET), Laboratorio de Ecología Evolutiva Humana, FACSO-UNCPBA, Quequén, Buenos Aires Province, Argentina
6. Instituto de Conservación de Ballenas, Buenos Aires, Argentina
7. School of Biological Sciences, University of Utah, Salt Lake City, Utah, United States
8. Department of Biology, University of Florida, Gainesville, Florida, United States
9. Department of Fisheries, Wildlife and Conservation Sciences, Oregon State University, Oregon, United States
10. Marine Evolution and Conservation Group, Groningen Institute of Evolutionary Life Sciences, University of Groningen, Groningen, The Netherlands
11. Centre for Coastal Studies, Provincetown, Massachusetts, United States
12. Laboratorio de Macroecología Marina, Centro de Investigación Científica y Educación Superior de Ensenada, Unidad La Paz, La Paz, México
13. Department of Natural Resources and Environment Tasmania, Hobart, Australia
14. Environmental Law Initiative, Wellington, New Zealand
15. School of Biological Sciences, University of Auckland Waipapa Taumata Rau, Auckland, New Zealand
16. Ecological Marine Services Pty. Ltd, Bundaberg, Queensland, Australia
17. Department of Natural History, NTNU University Museum, Norwegian University of Science and Technology, Trondheim, Norway
18. Núcleo de Gestão Integrada ICMBio Florianópolis (NGI ICMBio Florianópolis), Instituto Chico Mendes de Conservação da Biodiversidade (ICMBio), Ministério do Meio Ambiente, Florianópolis, Santa Catarina, Brazil
19. South Australian Research and Development Institute, Primary Industries and Regions South Australia, Adelaide, South Australia, Australia
20. School of Earth and Environmental Sciences, University of Adelaide, Adelaide, South Australia, Australia
21. Instituto Australis, Imbituba, Santa Catarina, Brazil
22. Stable Isotope Biogeochemistry Laboratory (SIBL), Department of Earth Sciences, Durham University, Durham, United Kingdom
23. School of Natural Sciences, Macquarie University, Sydney, NSW, Australia
24. Institute for Marine and Antarctic Studies, University of Tasmania, Tasmania, Australia

25. Department of Zoology, Faculty of Science, Charles University, Prague, Czech Republic
26. Department of Biology and Ecology, Faculty of Science, University of Ostrava, Ostrava, Czech Republic
27. British Antarctic Survey, Cambridge, United Kingdom
28. Cooperative Institute for Climate, Ecosystem and Ocean Studies, University of Washington & Marine Mammal Laboratory, Alaska Fisheries Science Center, NOAA
29. New Zealand Department of Conservation – Te Papa Atawhai, Wellington, New Zealand
30. Ivanhoe Sea Safaris, Gansbaai, South Africa
31. Dyer Island Conservation Trust, Great White House, Kleinbaai, South Africa
32. Grupo de Estudos de Mamíferos Aquáticos do Rio Grande do Sul, Torres, RS, Brazil
33. Laboratório de Ecologia de Mamíferos, Universidade do Vale do Rio dos Sinos, Sao Leopoldo, RS, Brazil
34. Universidade Estadual do Rio Grande do Sul, Osório, RS, Brazil
35. Collégial International Sainte-Anne, Montreal, Quebec, Canada
36. Ocean Alliance, Massachussetts, United States
37. Diversidad Biológica IV, Universidad Nacional de Córdoba, Córdoba, Argentina
38. Mammal Research Institute, Department of Zoology and Entomology, University of Pretoria, Pretoria, South Africa
39. Department Environment, Land Water and Planning, Warrnambool, Victoria, Australia
40. Marine Ecology and Telemetry Research & Cascadia Research Collective, United States

*Corresponding authors: Solène Derville and Emma L. Carroll, s.derville@live.fr, e.carroll@auckland.ac.nz

This PDF file includes:

Supporting text SI1 to SI4
Tables S1 to S5
Figures S1 to S14
Legends for Datasets S1 to S3
SI References

Other supporting materials for this manuscript include the following:

Datasets S1 to S3 in excel file

SI1. Multivariate analyses of southern right whale skin isotope data

We summarised the $\delta^{13}C$ and $\delta^{15}N$ values of SRW skin samples by wintering ground and decade (Supporting Dataset 1, Table S1). Note that Argentina was divided into high and low $\delta^{15}N$ values based on previous work (1). The overall dataset was significantly non-normal, based on the Shapiro-Wilks test ($\delta^{13}C$ W=0.922, p<0.001; $\delta^{15}N$ W = 0.787, p<0.001) run in R v 4.01 (2).

Table S1: Mean, standard deviation (SD), and range of $\delta^{13}C$ and $\delta^{15}N$ values of SRW skin samples by wintering ground and decade.

Wintering ground	Decade	n	Mean $\delta^{13}C$ (±SD) ‰	Range $\delta^{13}C$ ‰	Mean $\delta^{15}N$ (±SD) ‰	Range $\delta^{15}N$ ‰
Argentina - low	2000-2009	172	-21.3 (±0.9)	-23.9, -18.9	7.46 (±0.8)	6.0, 9.9
Argentina - high	2000-2009	40	-18.5 (±0.7)	-20.3, -17.2	12.4 (±1.14)	10.3, 15.0
Argentina	All	212	-20.8 (±1.4)	-23.9, -17.2	8.4 (±2.12)	6.0, 15.0
Brazil	1994-1999	7	-23.2 (±0.5)	-23.8, -22.6	7.4 (±0.9)	6.7, 9.3
Brazil	2000-2009	18	-22.2 (±0.9)	-23.5, -20.9	7.4 (±0.6)	6.5, 8.9
Brazil	All	25	-22.5 (±0.9)	-23.8, -20.9	7.4 (±0.7)	6.5, 9.3
South Africa	1994-1999	39	-23.8 (±1.2)	-26.0, -20.5	7.2 (±0.5)	6.5, 7.9
South Africa	2010-2020	78	-21.0 (±1.4)	-23.6, -16.3	7.1 (±1.3)	5.0, 12.2
South Africa	All	117	-21.9 (±1.9)	-26.0, -16.3	7.1 (±1.1)	5.0, 12.2
Southwest Australia	1994-1999	17	-22.8 (±1.9)	-25.1, -18.4	7.1 (±0.4)	6.2, 7.9
Southwest Australia	2000-2009	16	-21.1 (±1.7)	-23.4, -17.8	6.4 (±0.7)	5.6, 8.2
Southwest Australia	2010-2020	15	-20.5 (±0.9)	-21.8, -19.0	6.7 (±0.6)	5.9, 7.6
Southwest Australia	All	48	-21.9 (±1.9)	-25.1, -17.8	6.7 (±0.6)	5.6, 8.2
Southeast Australia	2000-2009	12	-20.2 (±1.2)	-22.4, -18.9	6.2 (±0.6)	5.3, 7.3
Southeast Australia	2010-2020	19	-21.9 (±1.3)	-24.1, -19.6	6.7 (±0.5)	5.4, 7.6
Southeast Australia	All	31	-21.2 (±1.6)	-24.1, 18.9	6.5 (±0.6)	5.3, 7.6
NZ Mainland	2000-2009	24	-20.0 (±1.1)	-23.3, -18.6	6.7 (±0.8)	5.0, 8.4
NZ Mainland	2010-2020	12	-21.0 (±1.3)	-23.4, -19.2	6.5 (±0.4)	5.9, 7.2
NZ Mainland	All	36	-20.4 (±1.2)	-23.4, 18.6	6.6 (±0.7)	5.0, 8.4
Auckland Islands	1990-1999	38	-18.7 (±0.8)	-21.6, -17.7	7.1 (±0.9)	5.8, 9.4
Auckland Islands	2000-2009	382	-19.2 (±0.6)	-22.2, -17.2	6.2 (±0.7)	4.6, 9.2
Auckland Islands	2010-2020	113	-19.6 (±0.4)	-21.5, -18.6	6.8 (±0.8)	5.1, 9.5
Auckland Islands	All	533	-19.3 (±0.6)	-22.2, -17.2	6.4 (±0.8)	4.6, 9.5

Kruskal–Wallis and post hoc Dunn's multiple comparison tests were used to assess differences in $\delta^{13}C$ and $\delta^{15}N$ values of whale skin with respect to wintering ground, decade and a combination of both wintering ground and decade. All Kruskal-Wallis tests were statistically significant for all comparisons: decade: $\delta^{13}C$ χ^2= 63.393, df = 2, p-value = 1.715e-14, $\delta^{15}N$ χ^2= 24.121, df = 2, p-value = 5.782e-06; wintering ground: $\delta^{13}C$ χ^2= 553.5, df = 7, p-value < 2.2e-16, $\delta^{15}N$ χ^2= 323.46, df = 7, p-value < 2.2e-16; wintering ground + decade: $\delta^{13}C$ χ^2= 630.64, df = 15, p-value < 2.2e-16, $\delta^{15}N$ χ^2= 392.66, df = 15, p-value < 2.2e-16. Decades were statistically significantly different in one if not both isotope systems (Table S2). Comparison of wintering grounds indicated that there was isolation by distance, with South American wintering grounds being significantly different to the New Zealand wintering grounds in both isotope systems. Regions that potentially share foraging grounds, such as South African and Australia (potentially Indian Ocean) and New Zealand and Australia (subtropical convergence south of Australia (3)), were not statistically distinct (Tables S3 and S4).

Table S2: Summary of $\delta^{13}C$ and $\delta^{15}N$ whale skin values and post hoc Dunn's test by decade. The left hand side includes the results of the post hoc Dunn's test result comparing overall wintering ground $\delta^{13}C$ and $\delta^{15}N$ whale skin values by decade, with z statistics with Bonferroni-corrected p-values in brackets with $\delta^{13}C$ in top right quadrant and $\delta^{15}N$ in bottom left quadrant; bolded values are statistically significant. The right hand side includes the mean, standard deviation (SD) and range for each isotope class by decade. Sample size shown by (n).

	Post hoc Dunn's test results			Mean ± SD (range)	
Decade (n)	1994-1999	2000-2009	2010-2020	$\delta^{13}C$	$\delta^{15}N$
1994-1999 (101)		**-5.96 (<0.001)**	-1.35 (0.530)	-21.7±2.6 (-26, -17.7)	7.1±0.7 (5.8, 9.4)
2000-2009 (664)	**4.86 (<0.001)**		**6.30 (<0.001)**	-19.9±1.3 (-23.9, -17.2)	7.0±1.7 (4.6, 15.0)
2010-2020 (237)	**3.35 (0.003)**	-1.61 (0.325)		-20.4±1.3 (-24.1, -16.3)	6.9±0.9 (5.0, 12.2)

Table S3: Post hoc Dunn's test results comparing $\delta^{13}C$ and $\delta^{15}N$ whale skin values by wintering ground. Shown are z statistics with Bonferroni-corrected p-values in brackets with $\delta^{13}C$ in top right quadrant and $\delta^{15}N$ in bottom left quadrant; bolded values are statistically significant.

	Argentina – high	Argentina – low	Brazil	South Africa	Southwest Australia	Southeast Australia	NZ mainland	Auckland Islands
Argentina – high		**12.10 (<0.001)**	**10.17 (0.001)**	**12.04 (<0.001)**	**9.27 (<0.001)**	**8.15 (<0.001)**	**6.53 (<0.001)**	**4.23 (<0.001)**
Argentina – low	**5.39 (<0.001)**		2.19 (0.801)	0.67 (1.00)	-0.85 (1.00)	-0.89 (1.00)	**-3.41 (0.018)**	**-16.31 (<0.001)**
Brazil	**3.75 (<0.001)**	0.04 (1.00)		-1.76 (1.00)	-2.46 (0.384)	-2.39 (0.476)	**-4.20 (0.001)**	**9.28 (<0.001)**
South Africa	**7.35 (<0.001)**	**3.34 (0.023)**	1.78 (1.00)		-1.28 (1.00)	-1.26 (1.00)	**3.70 (0.006)**	**14.80 (<0.001)**
Southwest Australia	**7.82 (<0.001)**	**4.45 (<0.001)**	2.91 (0.100)	1.91 (1.00)		0.15 (1.00)	2.20 (0.778)	**8.56 (<0.001)**
Southeast Australia	**7.99 (<0.001)**	**4.96 (<0.001)**	**3.57 (0.010)**	2.81 (0.139)	-1.04 (1.00)		1.84 (1.00)	-12.6 (1.00)
NZ mainland	**7.88 (<0.001)**	**4.71 (<0.001)**	**3.28 (0.029)**	-2.43 (0.423)	-0.62 (1.00)	0.43 (1.00)		**4.68 (<0.001)**
Auckland Islands	**12.75 (<0.001)**	**13.05 (<0.001)**	**-5.55 (<0.001)**	**-7.29 (<0.001)**	-2.77 (0.158)	-0.96 (1.00)	-1.63 (1.00)	

Table S4: Post hoc Dunn's test result comparing $\delta^{13}C$ and $\delta^{15}N$ whale skin values by wintering ground and decade. Shown are z statistics with Bonferroni-corrected p-values in brackets with $\delta^{13}C$ in top right quadrant and $\delta^{15}N$ in bottom left quadrant; bolded values are statistically significant. The abbreviations are as follows; 1990s for 1994-1999; 2000s for 2000-2009; 2010s for 2010-2020; ARG for Argentina, BRZ for Brazil, SAF for South Africa, SWA for Southwest Australia, SEA for Southeast Australia, MNZ for mainland NZ and AIS for Auckland Islands.

	BRZ 1990s	SAF 1990s	SWA 1990s	AIS 1990s	ARG high 2000s	ARG low 2000s	BRZ 2000s	SWA 2000s	SEA 2000s	MNZ 2000s	AIS 2000s	SAF 2010s	SWA 2010s	SEA 2010s	MNZ 2010s	AIS 2010s
BRZ 1990s		0.04 (1.000)	0.87 (1.000)	**6.58 (<0.001)**	**6.84 (<0.001)**	1.76 (1.000)	-0.66 (1.000)	-2.20 (1.000)	-3.09 (0.237)	-3.52 (0.053)	**5.73 (<0.001)**	-2.29 (1.000)	-2.43 (1.000)	-1.04 (1.000)	-1.87 (1.000)	**4.24 (0.003)**
SAF 1990s	0.22 (1.000)		-1.40 (1.000)	**11.94 (<0.001)**	**12.52 (<0.001)**	**3.91 (0.011)**	1.08 (1.000)	-3.41 (0.078)	**-4.50 (<0.001)**	**5.88 (<0.001)**	**13.09 (<0.001)**	**-4.70 (<0.001)**	**-3.71 (0.025)**	-1.70 (1.000)	2.74 (0.723)	**8.98 (<0.001)**
SWA 1990s	0.41 (1.000)	0.32 (1.000)		**7.93 (<0.001)**	**8.33 (<0.001)**	1.13 (1.000)	-0.29 (1.000)	-1.74 (1.000)	2.86 (0.501)	3.53 (0.051)	**7.23 (<0.001)**	1.20 (1.000)	-2.03 (1.000)	0.21 (1.000)	1.33 (1.000)	**4.85 (<0.001)**
AIS 1990s	-0.63 (1.000)	-0.74 (1.000)	-0.26 (1.000)		0.43 (1.000)	-11.30 (<0.001)	6.58 (<0.001)	5.73 (<0.001)	3.73 (0.023)	4.59 (<0.001)	3.06 (0.266)	9.10 (<0.001)	5.73 (<0.001)	7.99 (<0.001)	5.48 (<0.001)	5.61 (<0.001)
ARG high 2000s	2.59 (1.000)	**5.11 (<0.001)**	**4.29 (0.002)**	**5.82 (<0.001)**		**12.10 (<0.001)**	**8.85 (<0.001)**	**6.10 (<0.001)**	**4.04 (0.0064)**	**5.01 (<0.001)**	**3.72 (0.024)**	**9.76 (<0.001)**	**5.59 (<0.001)**	**8.41 (<0.001)**	**5.81 (<0.001)**	**6.25 (<0.001)**
ARG low 2000s	0.29 (1.000)	1.14 (1.000)	1.16 (1.000)	2.08 (1.000)	**5.39 (<0.001)**		1.56 (1.000)	-1.22 (1.000)	-2.66 (0.953)	**-3.81 (0.016)**	**-16.40 (<0.001)**	-1.66 (1.000)	-1.61 (1.000)	0.90 (1.000)	-0.71 (1.000)	**-8.04 (<0.001)**
BRZ 2000s	-0.32 (1.000)	0.82 (1.000)	0.97 (1.000)	-0.63 (1.000)	3.22 (0.153)	-0.13 (1.000)		-2.05 (1.000)	-3.16 (1.000)	-3.90 (1.000)	**7.85 (<0.001)**	-2.34 (1.000)	-2.34 (1.000)	-0.51 (1.000)	-1.61 (1.000)	**5.36 (<0.001)**
SWA 2000s	2.26 (1.000)	3.14 (0.201)	2.41 (1.000)	2.56 (1.000)	**7.04 (<0.001)**	**4.35 (0.002)**	3.40 (0.081)		1.24 (1.000)	1.59 (1.000)	**4.65 (<0.001)**	-0.34 (1.000)	-0.32 (1.000)	-1.58 (1.000)	-0.28 (1.000)	2.45 (1.000)
SEA 2000s	2.57 (1.000)	3.42 (0.074)	2.75 (0.708)	2.90 (0.444)	**6.93 (<0.001)**	**4.47 (0.001)**	**3.66 (0.030)**	-0.52 (1.000)		0.11 (1.000)	2.45 (1.000)	-1.82 (1.000)	0.90 (1.000)	2.74 (0.734)	-1.42 (1.000)	0.60 (1.000)
MNZ 2000s	1.52 (1.000)	-2.17 (1.000)	-1.48 (1.000)	1.51 (1.000)	**6.63 (<0.001)**	3.51 (0.054)	2.56 (1.000)	1.15 (1.000)	1.61 (1.000)		3.21 (0.162)	2.59 (1.000)	1.21 (1.000)	**3.42 (0.077)**	1.75 (1.000)	0.64 (1.000)
AIS 2000s	-3.23 (0.148)	**-6.79 (<0.001)**	-4.23 (0.003)	5.72 (<0.001)	**13.79 (<0.001)**	**14.64 (<0.001)**	-5.71 (1.000)	-0.82 (1.000)	-0.04 (1.000)	-2.76 (0.707)		**10.30 (<0.001)**	**4.08 (0.006)**	**7.33 (<0.001)**	**4.41 (0.001)**	**4.97 (<0.001)**
SAF 2010s	0.98 (1.000)	1.51 (1.000)	-0.76 (1.000)	0.64 (1.000)	**7.43 (<0.001)**	**3.66 (0.031)**	2.03 (1.000)	2.32 (1.000)	2.69 (0.856)	-1.14 (1.000)	**-6.81 (<0.001)**		-0.73 (1.000)	1.73 (1.000)	-0.05 (1.000)	**5.08 (<0.001)**
SWA 2010s	1.46 (1.000)	1.91 (1.000)	1.37 (1.000)	1.34 (1.000)	**5.71 (<0.001)**	2.900 (0.447)	2.33 (1.000)	-0.99 (1.000)	-1.43 (1.000)	0.05 (1.000)	-2.14 (1.000)	1.00 (1.000)		-1.88 (1.000)	-0.58 (1.000)	1.97 (1.000)
SEA 2010s	1.41 (1.000)	1.90 (1.000)	1.32 (1.000)	1.30 (1.000)	**6.04 (<0.001)**	**3.05 (0.001)**	2.34 (1.000)	1.18 (1.000)	-1.62 (1.000)	-0.09 (1.000)	-2.59 (1.000)	0.93 (1.000)	0.13 (1.000)		1.17 (1.000)	**4.81 (<0.001)**
MNZ 2010s	1.99 (1.000)	-2.69 (1.000)	-2.03 (1.000)	2.08 (1.000)	**6.10 (<0.001)**	**3.55 (0.046)**	2.93 (0.407)	0.19 (1.000)	0.67 (1.000)	0.83 (1.000)	-0.97 (1.000)	-1.81 (1.000)	-0.72 (1.000)	-0.88 (1.000)		2.51 (1.000)
AIS 2010s	-1.58 (1.000)	**-2.83 (<0.001)**	-1.66 (1.000)	1.90 (1.000)	**9.10 (<0.001)**	**6.01 (<0.001)**	2.99 (0.332)	1.53 (1.000)	1.99 (1.000)	0.17 (1.000)	**-5.76 (<0.001)**	-1.55 (1.000)	0.19 (1.000)	0.037 (1.000)	1.09 (1.000)	

SI2. UVic-MOBI model – data comparison and correction

2.1 Model Description

The Model of Ocean Biogeochemistry and Isotopes (MOBI) is coupled within the three dimensional ocean circulation component of the UVic Earth System Climate Model, version 2.9 (4). The latest version of MOBI-UVic model code is publicly available on GitHub (https://github.com/OSU-CEOAS-Schmittner/UVic2.9). MOBI predicts ^{13}C and ^{15}N isotope values in all respective model tracers including baseline dissolved inorganic nutrients, phytoplankton and zooplankton trophic levels (5, 6). The model is comprehensively described in the aforementioned publications (e.g., 7–11), and here we provide a brief description.

The two stable carbon isotopes, ^{12}C and ^{13}C, are included for dissolved inorganic carbon and organic carbon including phytoplankton, zooplankton, sinking particulate organic matter, and dissolved organic carbon. The most relevant processes determining the $\delta^{13}C$ distribution in the model include air-sea gas exchange, physical ocean transport, biological uptake and remineralization of organic carbon (see 10). To account for the Suess effect, a hindcast simulation with increasing atmospheric CO_2 and decreasing $\delta^{13}CO_2$ from atmospheric observations were applied to the model forcing, which results in a spatially varying Suess effect depending on the local ocean dynamics and biogeochemistry. For example, regions with strong upwelling and CO_2 outgassing to the atmosphere contain a smaller Suess effect than oceanic regions that have a net uptake of CO_2 from the atmosphere. In the Southern Ocean (30°S-80°S), the Suess effect lowers $\delta^{13}C$ in phytoplankton by 0.39‰ between years 1990 and 2020 on average, with the northernmost 10 degree section (30°S-40°S) experiencing 0.47‰ $\delta^{13}C$ decline, whereas the southernmost 10 degree section (70°S-80°S) experiencing only a 0.092‰ decline.

The two stable nitrogen isotopes, ^{14}N and ^{15}N, are included in nitrate and organic nitrogen including phytoplankton, zooplankton, sinking particulate organic matter, and dissolved organic nitrogen. The processes in the model that fractionate the nitrogen isotopes (i.e., preferentially incorporate ^{14}N into the product) are phytoplankton NO_3 assimilation (6‰), zooplankton excretion (4‰), N_2 fixation (-1‰), water column denitrification (22‰) and benthic denitrification (6‰), in which the respective fractionation factor yields the $\delta^{15}N$ difference between substrate and product (see 7). In the Southern Ocean, water column denitrification and N_2 fixation occur at insufficient rates to significantly affect the $\delta^{15}N$ distribution. Therefore, the nitrate utilization by phytoplankton drives the major meridional gradient of decreasing $\delta^{15}N$ values by 6‰ toward higher latitudes from 40°S to 75°S due to more iron- and light-limited phytoplankton growth.

2.2 Model-Data Correction

Recently, new marine particulate organic matter (POM) $\delta^{13}C$ and $\delta^{15}N$ data became available to better validate the MOBI model in the Southern Ocean. In particular, Verwega et al., (6) recently published the largest available marine $\delta^{13}C$ POM dataset, covering all major ocean basins since the 1960s, while St John Glew et al., (5) recently published a meta-analysis of all published surface POM $\delta^{13}C$ and $\delta^{15}N$ data for the Southern Ocean (for full information, refer to original publications). These new datasets were of particular interest to ensure that the model was performing in regions where such data have traditionally been sparse, but for which we were likely to need accurate information to assign foraging grounds, in particular, the Southern Ocean south of New Zealand and Australia.

To undertake the model-data comparison, we extracted the observational and MOBI-estimated values for $\delta^{13}C$ and $\delta^{15}N$ POM for 1.8° latitudinal bins from 78.3°S to 20.7°S, and calculated the same from the combined Verwega et al (6) and St John Glew et al (5) datasets. The observations and MOBI estimates were matched for season to ensure relevance to our analyses. Since the Suess effect is small in the Southern Ocean (0.39‰ in model, not detectable in observations due to high variance) compared to the meridional gradient (8.6‰, see Figure S13), we used all available seasonal data to maximize the amount of observations to validate and correct the model. Comparison of the seasonal mean values between the MOBI model and new datasets resulted in a correction by latitudinal bin that was incorporated into the isoscape assignment model. This model-data comparison revealed that the MOBI $\delta^{13}C$ consistently underestimated the zonally-averaged observations by 1.47‰ on average from 38°S to 80°S. Therefore, we corrected MOBI estimate by this amount (see Supporting Dataset 2). Since this correction is based on a zonal average, we introduced an additional error term to the assignment model calculated from the standard deviation of the model at each latitudinal bin, which was 0.52‰ on average (see section 3 below). Initial comparisons of the isoscape assignment model with the correction showed an improvement with the spatial overlap of the core feeding areas and whaling records by 8% on average across wintering grounds (and up to 27% for South Africa), which emphasizes the importance in validating model predictions with observations. The averaged $\delta^{15}N$ correction term was only 0.8‰ without a systematic bias and did not have a significant impact on the assignment model. The seasonal zonal mean values and correction by latitudinal bin are found in Supporting Dataset 2.

SI3. Isoscape Assignment Model

Isoscapes were constrained by wintering ground reflecting prior information on foraging and migration behavior of SRWs. Specifically, we constrained the isoscape to a ‘potential foraging range’ around each wintering ground that was limited to:
(1) latitudes < 30°S, as the species is distributed in oceans of the Southern Hemisphere, and historical catches are typically south of this latitude (12, 13);
(2) reflect the maximum swimming distance of SRWs in the five months prior to sampling (radius of 6500 km based on satellite track data analysis);
(3) >200 km away from the coast of Antarctica due to uncertainties in the isoscape model;
(4) Atlantic waters east of Navarino island (67°37’W) for South American foraging bubbles (Brazil and Argentina), as there is no evidence for a current use of the south Pacific Ocean by SRWs of the Atlantic breeding populations (14–16).

SRW skin isotope values were assigned to geographic regions of the isoscape using a bivariate-based assignment model (17). Assignments are made using both $\delta^{13}C$ for $\delta^{15}N$ values to estimate the likelihood that each raster cell in the isoscape represents the foraging area origin:

$$f(x, y|\mu_i, \Sigma) = \frac{1}{(2\pi\sigma_x\sigma_y\sqrt{1-\rho^2})}$$

$$\times \exp\left(-\frac{1}{1-\rho^2}\left[\frac{(x-\mu_x)^2}{\sigma_x^2} + \frac{(y-\mu_y)^2}{\sigma_y^2} + \frac{2\rho(x-\mu_x)(y-\mu_y)}{\sigma_x\sigma_y}\right]\right)$$

Where $f(x, y|\mu_i, \Sigma)$ is the likelihood that an individual with $\delta^{13}C$ value = x and $\delta^{15}N$ value = y originated from cell I with mean $\delta^{13}C$ and $\delta^{15}N$ values equal to the component in the vector μ_i and variance-covariance matrix Σ, which is decomposed on the right hand side of the equation such that ρ is the correlation between $\delta^{13}C$ and $\delta^{15}N$ values in the overall dataset (0.16), and where σ_x^2 is the pooled error in $\delta^{13}C$ values, and σ_y^2 is the pooled error in $\delta^{15}N$ values.

The pooled error comes from several sources, and is defined differently here than in (17):

$$\sigma_{pool} = \sqrt{\sigma_i + \sigma_{t1} + \sigma_{t2} + \sigma_r}$$

Where σ_i is the within-individual error, estimated from running replicate samples of the same individual (0.5‰ for $\delta^{13}C$ and 0.4‰ for $\delta^{15}N$, Supporting Dataset 3); where $\sigma_{t1}$and σ_{t2} are the variance in TDFs at each trophic level increase (for phytoplankton to zooplankton we conservatively used 0.3‰ for both $\delta^{13}C$ and $\delta^{15}N$; for zooplankton to whale we used: 0.4‰ for $\delta^{13}C$ and 0.3‰ for $\delta^{15}N$ (18)); and where σ_r is the variance per pixel in the isoscape across months used in the analysis (standard deviation calculated from the third to the fifth months prior to sampling). The estimate of σ_i was derived from analyses of technical replicates (samples split and run separately) and whales resampled within the same 2-3 week field season; the distribution of differences between technical replicates and field resamples were not statistically different so were pooled to give the within-individual variation estimate (Supporting Dataset 3).

SI4. Validation of the Trophic Discrimination Factor (TDF)

Measurements of consumer $\delta^{13}C$ and $\delta^{15}N$ values are different from those of their prey. This difference in isotope ratios is often referred to as the trophic discrimination factor (TDF, written $\Delta^{13}C$ and $\Delta^{15}N$ for carbon and nitrogen, respectively). We used satellite track data from SRWs to validate the TDFs used in our isoscape assignment model. First, we reviewed the literature for a range of potential $\Delta^{13}C$ and $\Delta^{15}N$ TDFs. Meta-analyses (19–21) indicated that TDFs range from 0–2‰ for $\Delta^{13}C$ and 2–5‰ for $\Delta^{15}N$ and can vary among consumer tissue types, dietary nutritional quality, and nitrogen excretion pathway (e.g., ammonia or urea). Zooplankton mean TDFs are ~2.0±0.5‰ for $\Delta^{13}C$ and 2.5±0.5‰ for $\Delta^{15}N$ (22, 23). TDFs for baleen whales have been estimated to be 1.3±0.4‰ for $\Delta^{13}C$ and between 1.8±0.3‰ and 2.8±0.3‰ for $\Delta^{15}N$ (18, 24). Based on these patterns, we selected a range of TDFs of 2–4‰ for $\Delta^{13}C$ and 4–6‰ for $\Delta^{15}N$ (in 0.5‰ increments) to account for the two trophic levels between the phytoplankton baseline isoscape and SRW (secondary consumers) skin tissue.

We then compiled SRW satellite track data for 49 individuals tagged with Argos-linked satellite tags (SPOT5, SPOT6 and SPLASH10, Wildlife Computers) in two winter breeding grounds (Argentina, n=31 (14, 16, 25), and Auckland Islands, n=16 (26)) and one summer foraging ground (South Georgia, n=2 (27)). For the Auckland Islands and South Georgia data, state-space models were used to define area restricted search (ARS) behavior, indicative of likely foraging. ARGOS locations incorporate a measure of error represented by seven accuracy classes (in descending order: 3, 2, 1, 0, A, B, and Z, (28). We filtered the data to remove invalid locations of class Z and locations implying unrealistically rapid movements (speed > 5 m/s). We calculated the maximum swimming distance away from the breeding grounds in the five months prior to sampling to be used as a range constraint in the isoscape assignment (see SI3). Whenever a track was interrupted for more than 6 days, it was considered to contain several segments. Segments containing less than 15 locations were removed, while the rest were interpolated at one position every 6 hours with a random walk state-space model using the *foieGras* R package (version 0.7-6 (29)). The dataset had an average of one Argos position every 1.4 hours (SD 6.9 hours), supporting the 6-hour time step. This approach considers the different spatial accuracies associated with each ARGOS location and derives a metric of move persistence γ at each predicted position. Move persistence ranges from γ=0 (area restricted movement) to γ=1 (directed movement) and was used to define ARS indicative of potential foraging behavior. The positions estimated with the 50 % lowest γ values were classified as ARS positions. Argentinean data were provided as ARS locations following comparable methods (25) and are visible on Figure 5 of that reference; data from New Zealand and South Georgia analysed here were filtered in the same way and ARS classification followed a similar approach. ARS positions were aggregated over a grid that matched with the phytoplankton Model of Ocean Biogeochemistry and Isotopes (MOBI (8, 11)) in resolution and extent, which is more coarse than typical movement ecology studies (30). Raster cells that were categorized as ARS behavior but located less than 20 km from a coast at breeding latitudes were removed to ensure that those ARS points were not due to breeding/socializing (31, 32) or nursing/calving behavior (33, 34).

To optimize TDF selection, we iteratively fitted the isoscape assignment models with different TDF combinations to $\delta^{13}C$ and $\delta^{15}N$ values of SRW skin samples acquired in wintering grounds where satellite tracking had been collected as well (Auckland Islands n = 533 samples and Argentina n = 212 samples). In total, we fitted 25 different models, each with a unique combination of TDF values, to identify probable foraging areas using the assignment model described in SI3. The TDF values that produced the geographic assignments with the highest percentage overlap with the ARS data were identified for each region. To assign Argentinean samples, we used the ARS data from both the Argentinean and South Georgia satellite tracks, given the migratory and genetic links between these regions (35). We averaged the best-fitting TDFs from the Auckland Islands and Argentinean data to generate one value each for $\Delta^{13}C$ and for $\Delta^{15}N$ to apply across the whole SRW skin dataset.

The TDF values that maximized the number of ARS locations overlapping with isotopically assigned foraging areas were 2‰ for $\Delta^{13}C$ and 5‰ for $\Delta^{15}N$ in the Argentinean samples and 4‰ for $\Delta^{13}C$ and 4.5‰ for $\Delta^{15}N$ in the Auckland Islands samples. The average between the best-fitting TDFs was equal to 3‰ for $\Delta^{13}C$ and 4.8‰ for $\Delta^{15}N$. Only the assignments generated with this optimal TDF setting are presented hereafter.

We took the approach outlined above due to the temporal mismatch between the information on foraging grounds provided by isotope data from skin biopsy samples collected on wintering grounds and satellite telemetry information from whales tagged on these same wintering grounds. Due to the isotopic turnover rate, the skin biopsy samples represent the foraging of the whales in late summer to autumn (24). In contrast, the satellite tags are deployed in winter, and typically last 3-6 months, that is, until spring to summer (36, 37). Therefore, the skin biopsy samples collected from satellite tagged whales do not reflect the same foraging period as the tracking data.

Supporting Datasets

Supporting Dataset 1: Stable isotope values for whale skin samples used in this analysis.

Supporting Dataset 2: Latitudinal bin correction that was incorporated into the isoscape assignment model using the model-data comparison described in SI2.

Supporting Dataset 3: Information used to estimate within-individual variation in stable isotope values for whale skin data. This is based on replicate analysis of skin biopsy samples. Shown are the sample ID, whale ID, $\delta^{13}C$ and $\delta^{15}N$ values, % carbon (C) and nitrogen (N) and C/N ratio for each replicate. Differences between the replicates are shown in the delta values column.

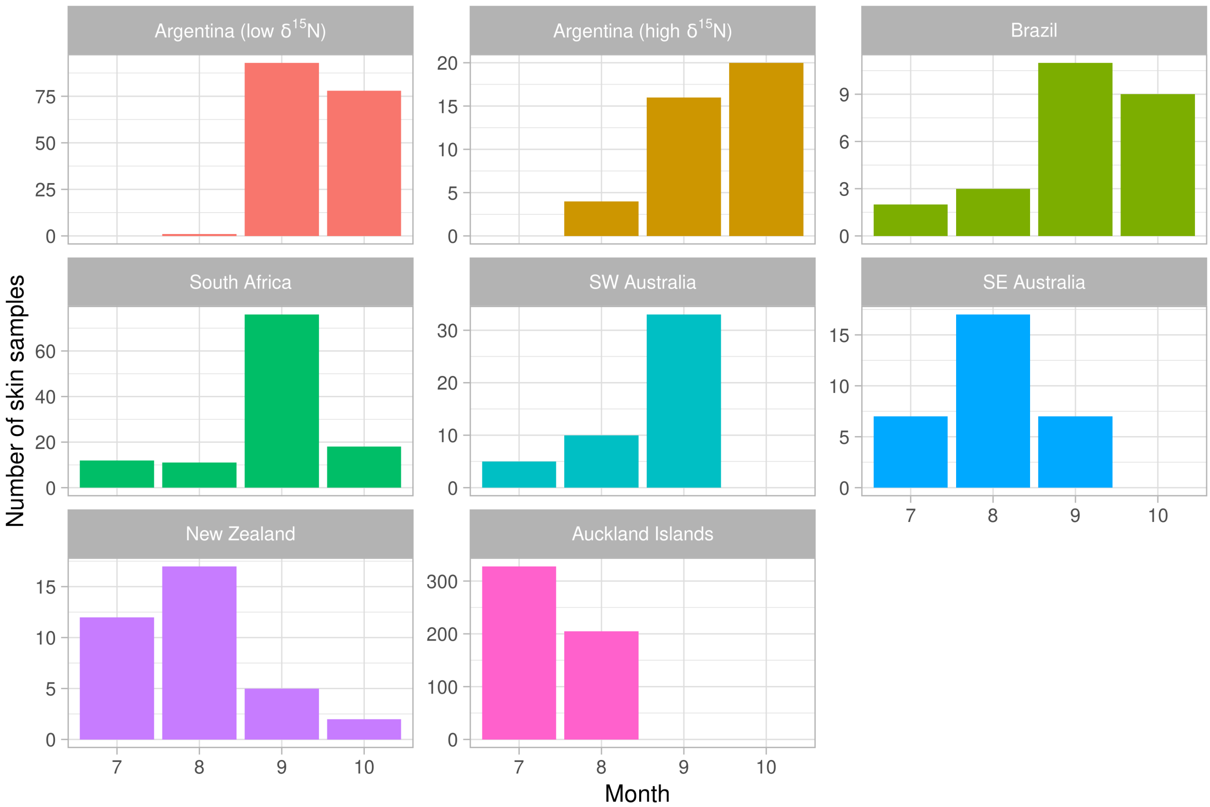

Figure S1. Temporal distribution of SRW skin samples across collection months (July to October) and wintering grounds. Note that the ranges of the y-axis vary by panel. In addition, whales arrive and calve earlier in New Zealand and Australia, which explains the difference in the sampling time frames compared to other wintering grounds.

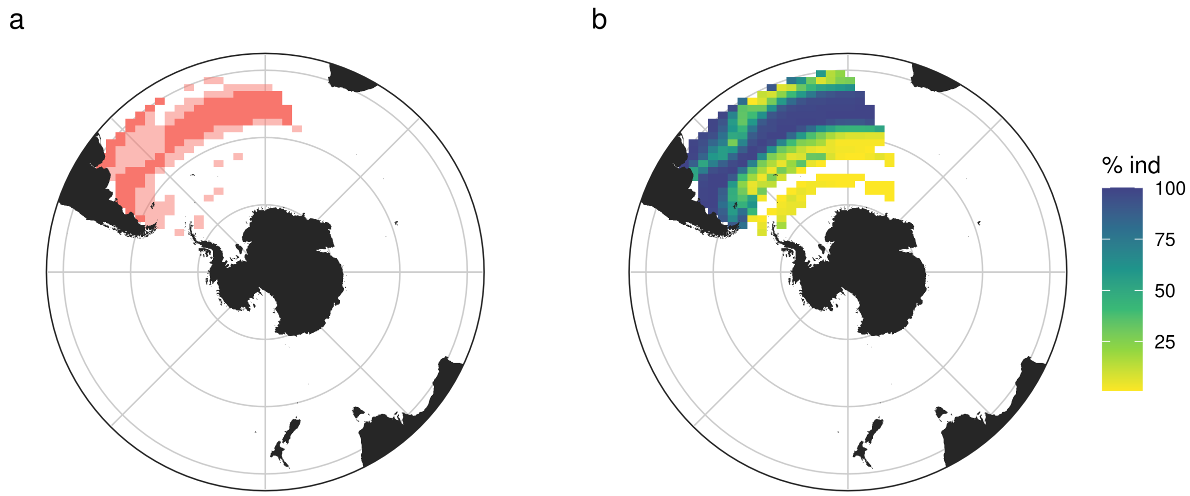

Figure S2. Isotopically assigned foraging grounds for southern right whales sampled in Argentina and presenting low $\delta^{15}N$ values. (a) Population-level average core and general foraging areas in dark and light colors, respectively. (b) Individual-level general foraging grounds shown with a color scale representing the percent of sampled individuals whose general foraging ground overlapped over a grid cell.

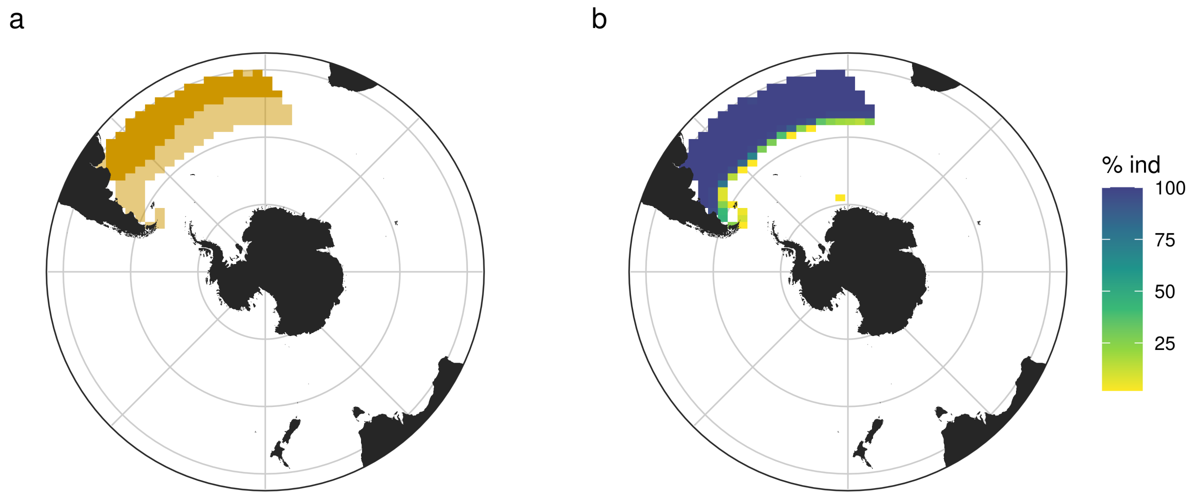

Figure S3. Isotopically assigned foraging grounds for southern right whales sampled in Argentina and presenting high $\delta^{15}N$ values. (a) Population-level average core and general foraging areas in dark and light colors, respectively. (b) Individual-level general foraging grounds shown with a color scale representing the percent of sampled individuals whose general foraging ground overlapped over a grid cell.

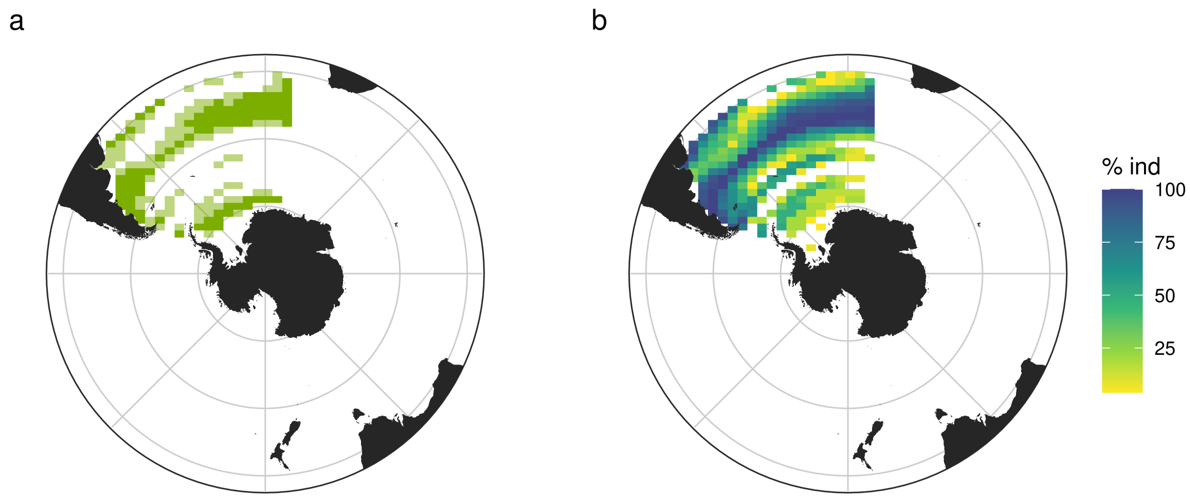

Figure S4. Isotopically assigned foraging grounds for southern right whales sampled in Brazil. (a) Population-level average core and general foraging areas in dark and light colors, respectively. (b) Individual-level general foraging grounds shown with a color scale representing the percent of sampled individuals whose general foraging ground overlapped over a grid cell.

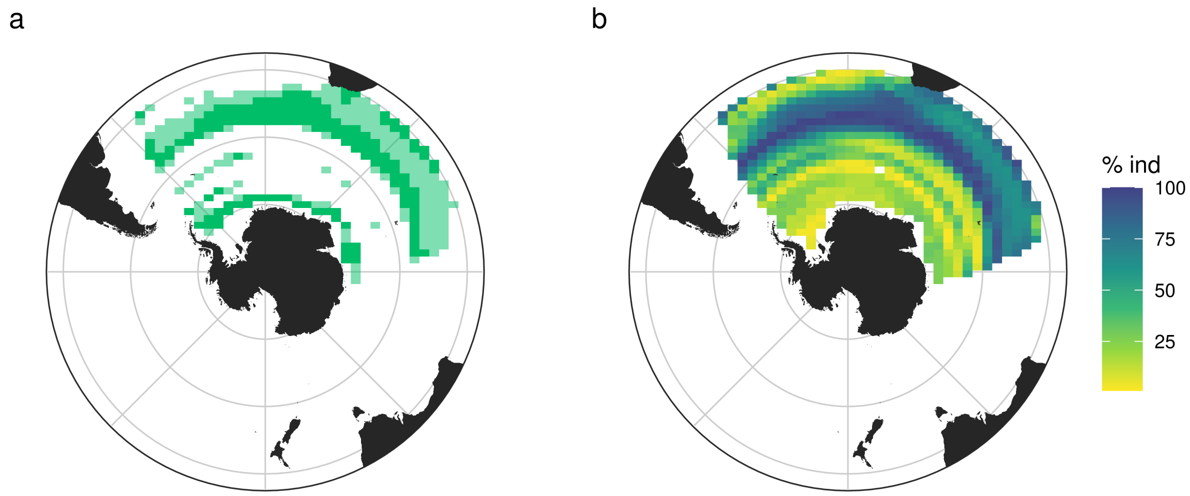

Figure S5. Isotopically assigned foraging grounds for southern right whales sampled in South Africa. (a) Population-level average core and general foraging areas in dark and light colors, respectively. (b) Individual-level general foraging grounds shown with a color scale representing the percent of sampled individuals whose general foraging ground overlapped over a grid cell.

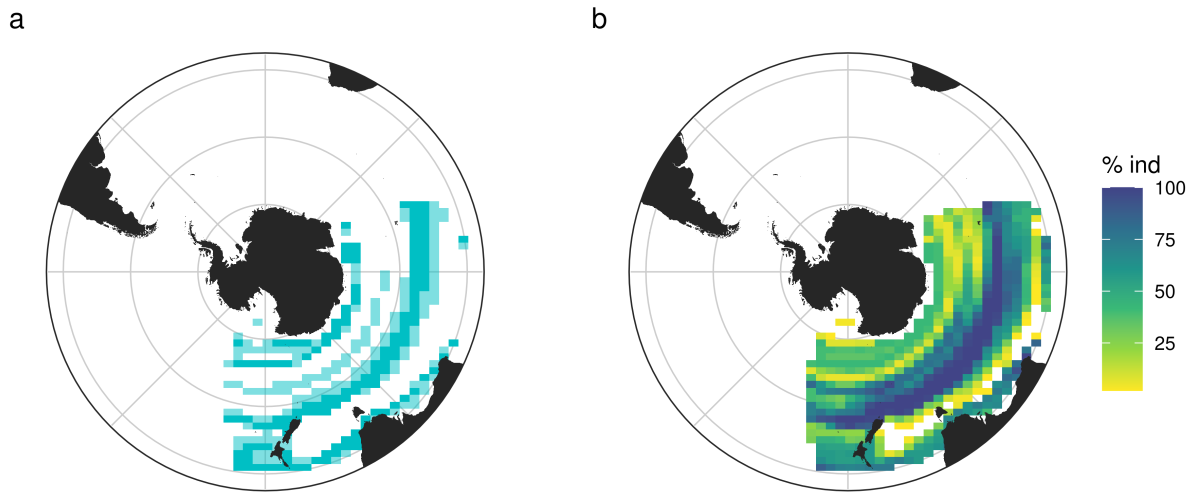

Figure S6. Isotopically assigned foraging grounds for southern right whales sampled in Southwest Australia. (a) Population-level average core and general foraging areas in dark and light colors, respectively. (b) Individual-level general foraging grounds shown with a color scale representing the percent of sampled individuals whose general foraging ground overlapped over a grid cell.

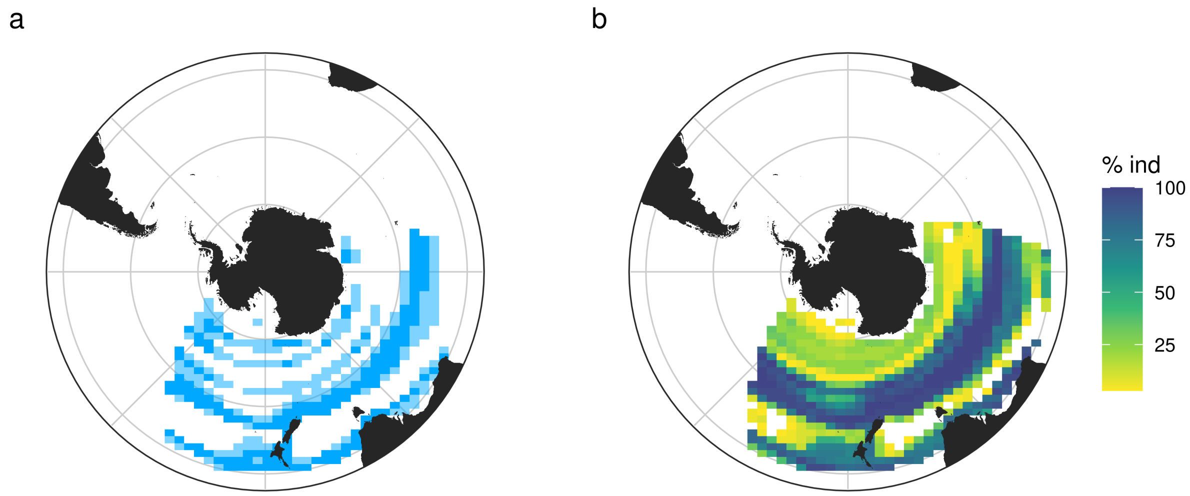

Figure S7. Isotopically assigned foraging grounds for southern right whales sampled in Southeast Australia. (a) Population-level average core and general foraging areas in dark and light colors, respectively. (b) Individual-level general foraging grounds shown with a color scale representing the percent of sampled individuals whose general foraging ground overlapped over a grid cell.

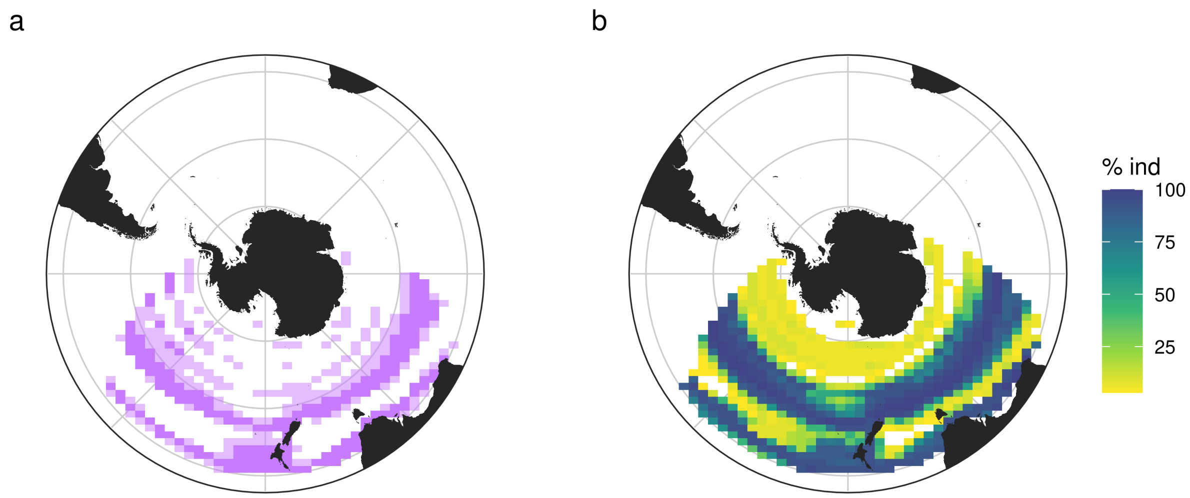

Figure S8. Isotopically assigned foraging grounds for southern right whales sampled in New Zealand. (a) Population-level average core and general foraging areas in dark and light colors, respectively. (b) Individual-level general foraging grounds shown with a color scale representing the percent of sampled individuals whose general foraging ground overlapped over a grid cell.

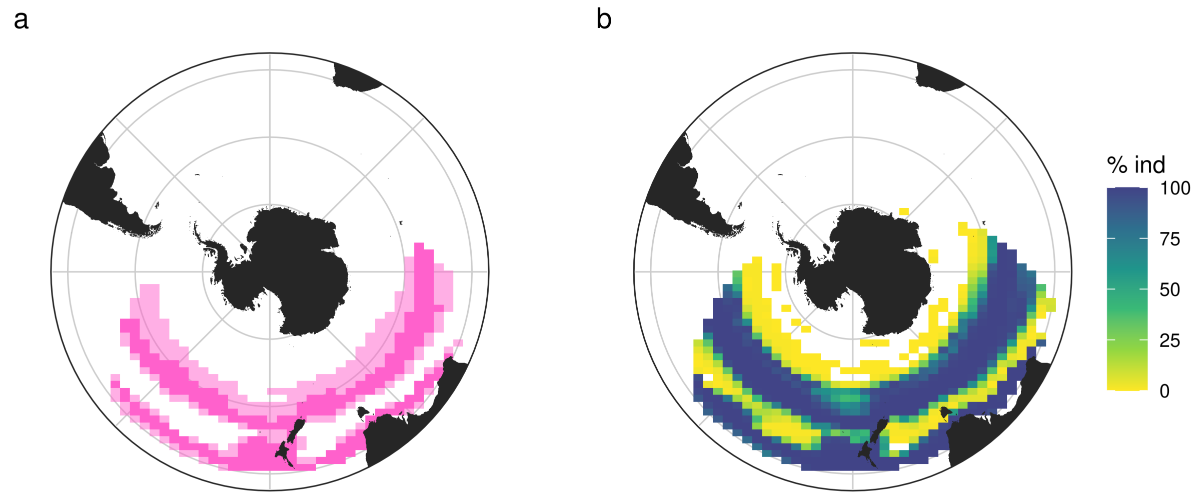

Figure S9. Isotopically assigned foraging grounds for southern right whales sampled in the Auckland Islands. (a) Population-level average core and general foraging areas in dark and light colors, respectively. (b) Individual-level general foraging grounds shown with a color scale representing the percent of sampled individuals whose general foraging ground overlapped over a grid cell.

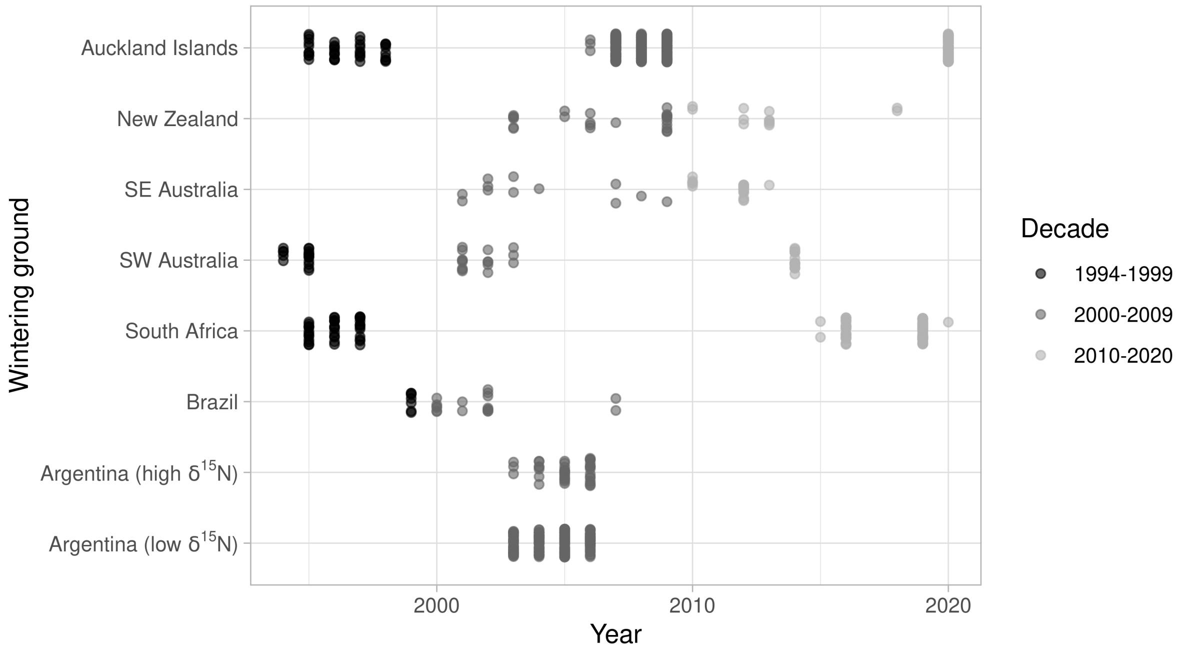

Figure S10. Temporal distribution of southern right whale skin samples collected across decades in seven different wintering grounds (high and low $\delta^{15}N$ Argentinean groups are split).

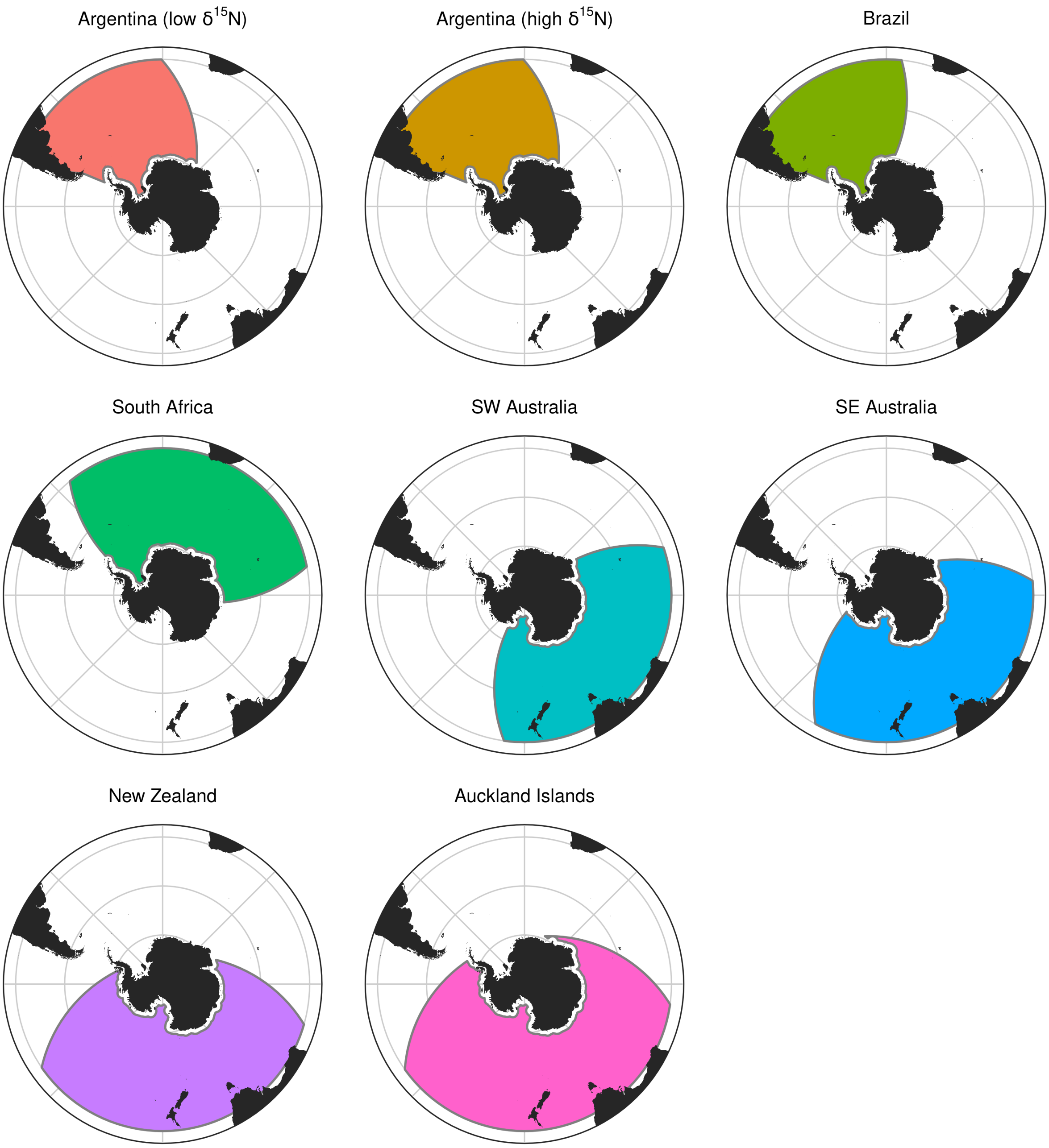

Figure S11. Foraging bubbles representing the potential foraging range for each southern right whale wintering ground considered in this study.

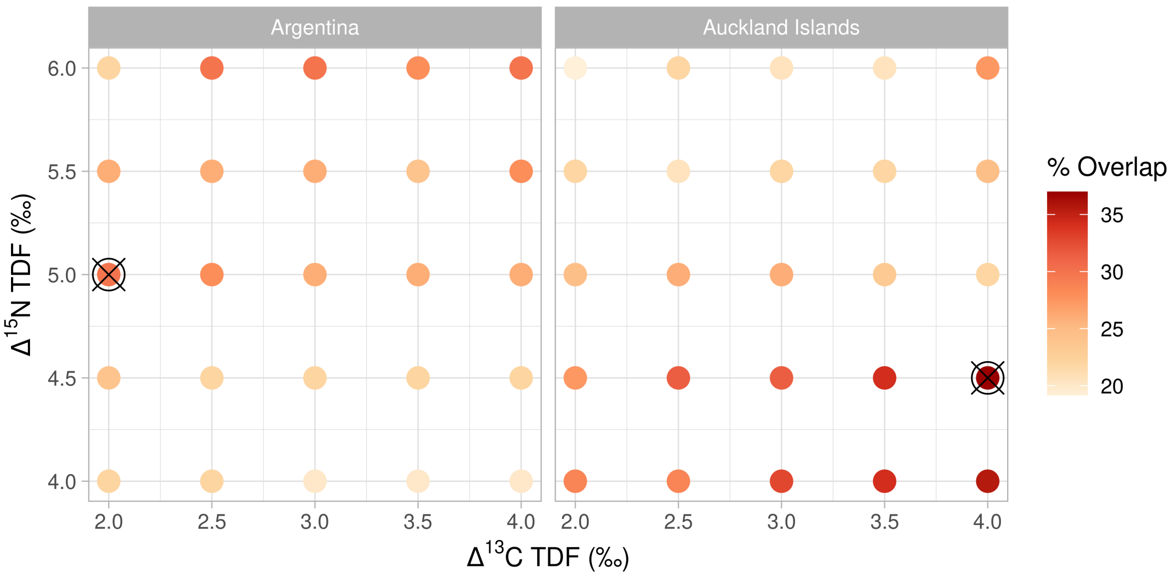

Figure S12. Results of iterative assignments to identify the best-fitting TDFs using the Auckland Islands and Argentinean samples. The percent of overlap between the isotopically assigned general foraging areas and the foraging locations identified in satellite tracks is represented on a colored scale. The TDFs that generated the highest percent overlap per wintering ground are indicated by a black cross.

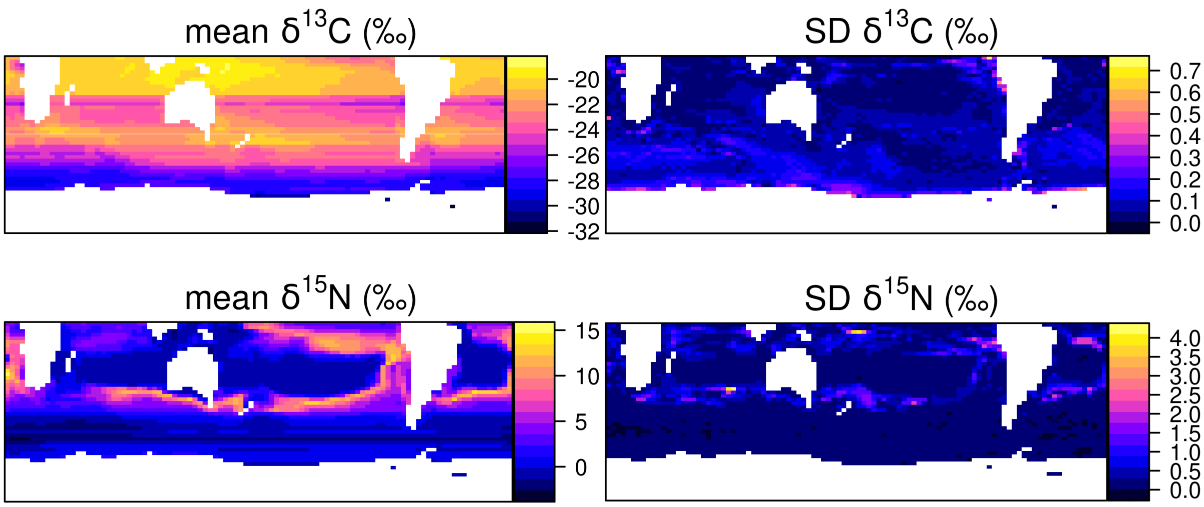

Figure S13. Baseline data-constrained (6, 38) phytoplankton isoscape mean and standard deviation (SD) calculated over the third to the fifth months prior to sampling (example presented for a skin sample collected in South Africa in August 1995) from the most recent version (9) of the Model of Ocean Biogeochemistry and Isotopes (8).

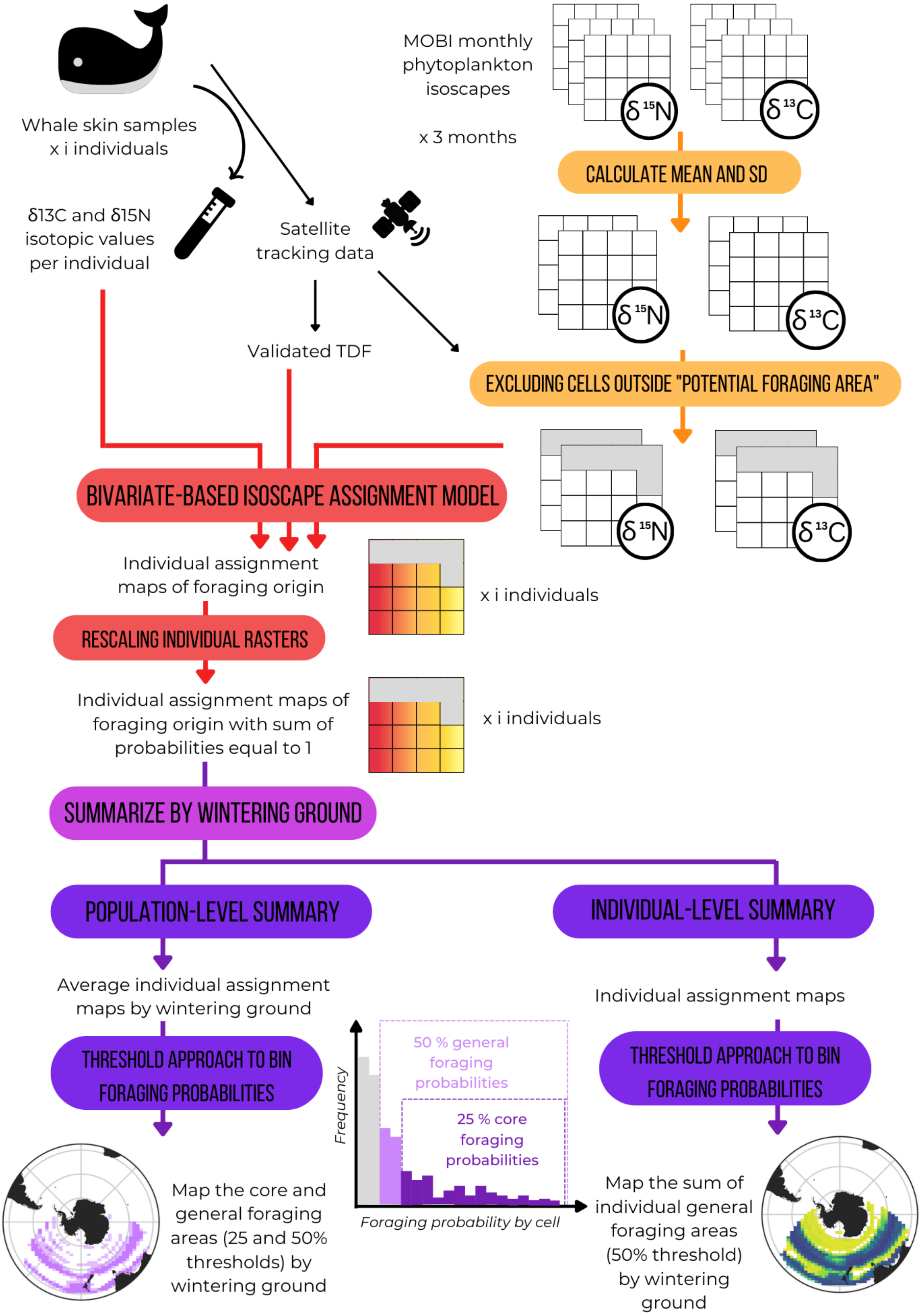

452
453 **Figure S14.** Schematic representation of the isotopic assignment modelling approach.

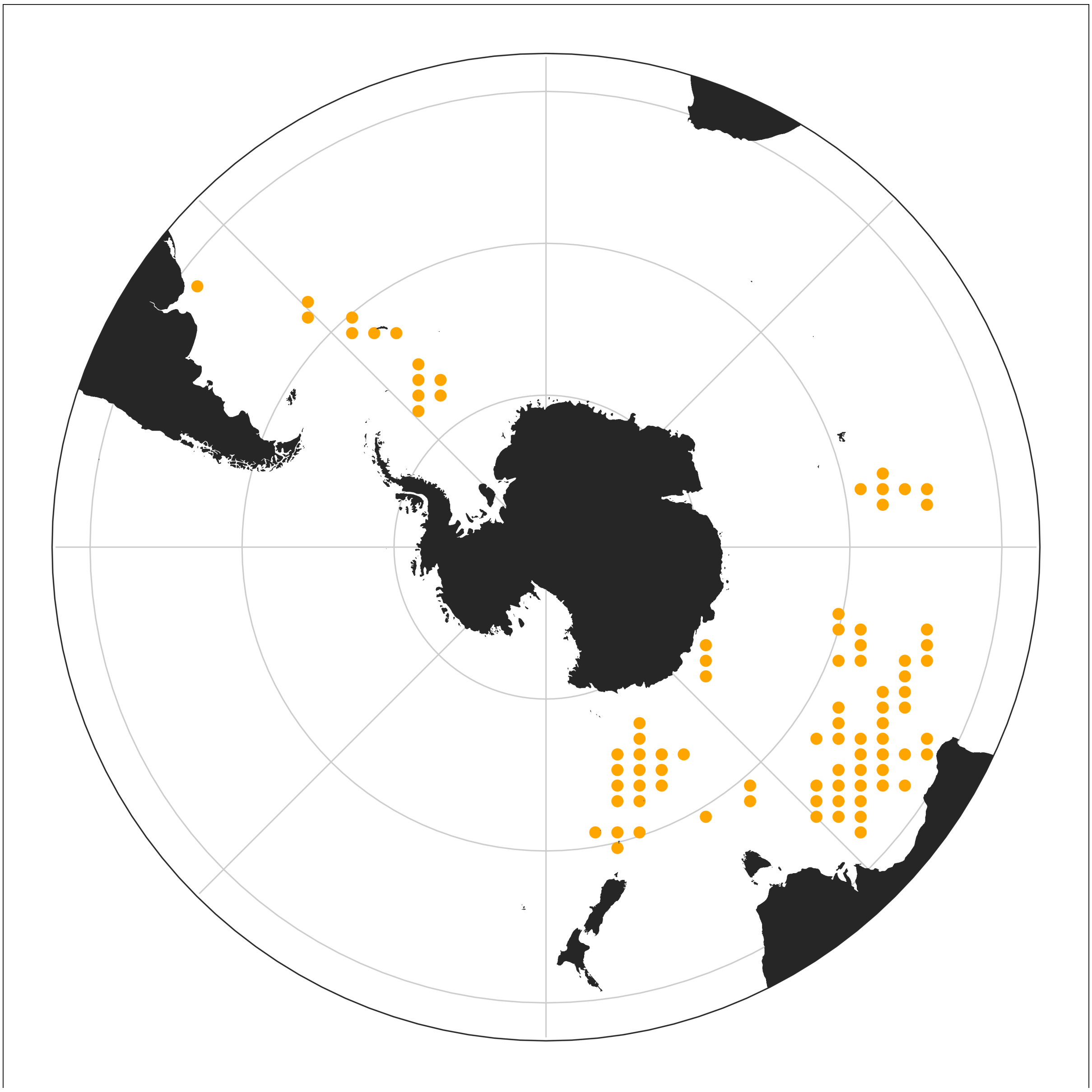

Figure S15. Area restricted search (ARS) locations (n = 123), assumed to be foraging ground locations, for southern right whales satellite tagged at the Auckland Islands and South Georgia. ARS locations result from the spatial aggregation of 9,016 interpolated satellite tracking positions estimated to show ARS behaviour.

Table S5. Information on stable isotope analyses, including lipid extraction method, instruments and standards used, and citations if data are drawn from publications. All studies used Vienna Pee Bee Belemnite for carbon and atmospheric air for nitrogen as standards. n = sample size, Ref = reference.

	n	Lipid extraction method	Instruments/Location	Standards	Reference
Argentina	212	(39)	Carlo Erba 1108 Elemental Analyzer coupled to a ThermoFinnigan Delta S IRMS at the Stable Isotope Ratio Facility for Environmental Research (SIRFER) at the University of Utah	Laboratory reference materials (2 glutamic acids) were + 24.0 and + 49.6 ‰ for UU-CN-1, −28.2 and −4.6 ‰ for UU-CN-2, respectively, and $\delta^{13}C$ and $\delta^{15}N$ values of a powdered keratin quality control material were −24.0 and + 5.9 ‰, respectively. These values were assigned after calibration against the international standards USGS40 and USGS41.	(1, 40, 41)
Brazil	25	(39)	Costech Elemental Analyser (ECS 4010) coupled to a ThermoFinnigan Delta V Advantage isotope ratio mass spectrometer, Durham University Stable Isotope Biogeochemistry Laboratory	USGS 40, USGS 24, IAEA 600, IAEA N1, IAEA N2	This paper; (42)

South Africa	117	(39)	Costech Elemental Analyser (ECS 4010) coupled to a ThermoFinnigan Delta V Advantage isotope ratio mass spectrometer, Durham University Stable Isotope Biogeochemistry Laboratory and Delta V Plus stable light isotope ratio mass spectrometer via a ConFlo IV system, housed at the Stable Isotope Laboratory, Mammal Research Institute, University of Pretoria	Merck Gel: $\delta^{13}C = -20.3‰$, $\delta^{15}N = 7.9‰$, C% = 41.3, N% = 15.3 and DL-Valine: $\delta^{13}C = -10.6‰$, $\delta^{15}N = -6.2‰$, C% = 55.5, N% = 11.9), which were calibrated against international standards (NBS 22, IAEA-CH-3, IAEA-CH-6, IAEA-CH-7, IAEA N-1, IAEA N-2, IAEA NO-3	This paper; (43)
Southwest Australia	48	(39)	Costech Elemental Analyser (ECS 4010) coupled to a ThermoFinnigan Delta V Advantage isotope ratio mass spectrometer, Durham University Stable Isotope Biogeochemistry Laboratory	USGS 40, USGS 24, IAEA 600, IAEA N1, IAEA N2	This paper; (44)
Southeast Australia	31	(39)	Costech Elemental Analyser (ECS 4010) coupled to a ThermoFinnigan Delta V Advantage isotope ratio mass spectrometer, Durham University Stable Isotope Biogeochemistry Laboratory	USGS 40, USGS 24, IAEA 600, IAEA N1, IAEA N2	(44)
New Zealand Mainland	36	(24)	Costech 4010 Elemental Analyzer coupled to a Thermo Scientific Delta V isotope ratio mass spectrometer at the University of Wyoming Stable Isotope Facility	USGS 40, IAEA 600, IAEA N2	This paper; (42)
Auckland Islands	533	(24)	Costech 4010 Elemental Analyzer coupled to a Thermo Scientific Delta V isotope ratio mass spectrometer at the University of Wyoming Stable Isotope Facility; University of New Mexico	USGS 40, IAEA 600, IAEA N2	This paper; (42)

SI references

1. L. O. Valenzuela, V. J. Rowntree, M. Sironi, J. Seger, Stable isotopes in skin reveal diverse food sources used by southern right whales (*Eubalaena australis*). *Mar. Ecol. Prog. Ser.* **603**, 243–255 (2018).
2. R Core Team, "R: A language and environment for statistical computing. R Foundation for Statistical Computing, Vienna, Austria. URL https://www.R-project.org/" (2021).
3. A. I. Mackay, *et al.*, Satellite derived offshore migratory movements of southern right whales (*Eubalaena australis*) from Australian and New Zealand wintering grounds. *PLoS One* **15**, e0231577 (2020).
4. M. Eby, *et al.*, Lifetime of anthropogenic climate change: Millennial time scales of potential CO2 and surface temperature perturbations. *J. Clim.* **22**, 2501–2511 (2009).
5. K. St John Glew, *et al.*, Seasonality in Southern Ocean isoscapes (2020).
6. M. T. Verwega, *et al.*, Description of a global marine particulate organic carbon-13 isotope data set. *Earth Syst. Sci. Data* **13**, 4861–4880 (2021).
7. C. J. Somes, *et al.*, Simulating the global distribution of nitrogen isotopes in the ocean. *Global Biogeochem. Cycles* **24**, 1–16 (2010).
8. A. Schmittner, C. J. Somes, Complementary constraints from carbon (^{13}C) and nitrogen (^{15}N) isotopes on the glacial ocean's soft-tissue biological pump. *Paleoceanography* **31**, 669–693 (2016).
9. C. J. Somes, *et al.*, Constraining Global Marine Iron Sources and Ligand-Mediated Scavenging Fluxes With GEOTRACES Dissolved Iron Measurements in an Ocean Biogeochemical Model. *Global Biogeochem. Cycles* **35**, e2021GB006948 (2021).
10. A. Schmittner, *et al.*, Biology and air-sea gas exchange controls on the distribution of carbon isotope ratios (δ13C) in the ocean. *Biogeosciences* **10**, 5793–5816 (2013).
11. C. J. Somes, A. Schmittner, J. Muglia, A. Oschlies, A three-dimensional model of the marine nitrogen cycle during the last glacial maximum constrained by sedimentary isotopes. *Front. Mar. Sci.* **4**, 1–24 (2017).
12. T. D. Smith, R. R. Reeves, E. Josephson, J. N. Lund, Spatial and seasonal distribution of American whaling and whales in the age of sail. *PLoS One* **7**, e34905. doi:10.1371/journal.pone.0034905 (2012).
13. D. Tormosov, *et al.*, Soviet catches of Southern right whales *Eubalaena australis* 1951-1971. *Biol. Conserv.* **86**, 185–197 (1998).
14. A. Zerbini, *et al.*, Tracking southern right whales through the southwest Atlantic : An update on movements , migratory routes and feeding grounds. *Rep. SC/66a/BRG22 Present. to Sci. Comm. Int. Whal. Comm. Cambridge, UK. Available from https//iwc.int*, 1–15 (2016).
15. P. Best, R. Payne, V. J. Rowntree, J. Palazzo, M. Both, Long-range movements of South Atlantic right whales *Eubalaena australis*. *Mar. Mammal Sci.* **9**, 227–234 (1993).
16. A. N. Zerbini, *et al.*, Tracking southern right whales through the southwest Atlantic: new insights into migratory routes and feeding grounds. *Rep. SC/66b/BRG26 Present. to Sci. Comm. Int. Whal. Comm. Cambridge, UK. Available from https//iwc.int*, 1–15 (2015).
17. H. B. Vander Zanden, *et al.*, Determining origin in a migratory marine vertebrate: A novel method to integrate stable isotopes and satellite tracking. *Ecol. Appl.* **25**, 320–335 (2015).
18. A. Borrell, N. Abad-Oliva, E. Gõmez-Campos, J. Giménez, A. Aguilar, Discrimination of stable isotopes in fin whale tissues and application to diet assessment in cetaceans.

Rapid Commun. Mass Spectrom. **26**, 1596–1602 (2012).
19. J. H. McCutchan, W. M. Lewis, C. Kendall, C. C. McGrath, Variation in trophic shift for stable isotope ratios of carbon, nitrogen, and sulfur. *Oikos* **102**, 378–390 (2003).
20. S. Caut, E. Angulo, F. Courchamp, Variation in discrimination factors ($\Delta^{15}N$ and $\Delta^{13}C$): The effect of diet isotopic values and applications for diet reconstruction. *J. Appl. Ecol.* **46**, 443–453 (2009).
21. M. A. Vanderklift, S. Ponsard, Sources of variation in consumer-diet $\delta^{15}N$ enrichment: A meta-analysis. *Oecologia* **136**, 169–182 (2003).
22. P. Tiselius, K. Fransson, Contribution to the Themed Section : ' The Role of Zooplankton in Marine Biogeochemical Cycles : From Fine Scale to Global Daily changes in d N and d C stable isotopes in copepods : equilibrium dynamics and variations of trophic level in the field. **38**, 751–761 (2016).
23. C. Mompeán, A. Bode, E. Gier, M. D. McCarthy, Bulk vs. amino acid stable N isotope estimations of metabolic status and contributions of nitrogen fixation to size-fractionated zooplankton biomass in the subtropical N Atlantic. *Deep. Res. Part I Oceanogr. Res. Pap.* **114**, 137–148 (2016).
24. G. Busquets-Vass, *et al.*, Estimating blue whale skin isotopic incorporation rates and baleen growth rates: Implications for assessing diet and movement patterns in mysticetes. *PLoS One* **12**, e0177880 (2017).
25. A. N. Zerbini, *et al.*, Satellite tracking of Southern right whales (*Eubalaena australis*) from Golfo San Matías, Rio Negro Province, Argentina. *Rep. SC/67b/CMP17 to Sci. Comm. Int. Whal. Comm. Cambridge, UK. Available from https//iwc.int* (2018).
26. E. L. Carroll, *et al.*, Satellite tracking and genetic evidence of changing migratory traditions after exploitation. *prep.*
27. A. Kennedy, *et al.*, Photo-ID and satellite tracking connects South Georgia (Islas Georgias del Sur) southern right whales with multiple feeding and calving grounds in the southwest Atlantic. *Mar. Mammal Sci.*
28. D. G. Nicholls, C. J. Robertson, M. D. Murray, Measuring accuracy and precision for CLS: Argos satellite telemetry locations. *Notornis* **54**, 137–157 (2007).
29. I. D. Jonsen, *et al.*, A continuous-time state-space model for rapid quality control of argos locations from animal-borne tags. *Mov. Ecol.* **8**, 31 (2020).
30. R. R. Reisinger, *et al.*, Habitat model forecasts suggest potential redistribution of marine predators in the southern Indian Ocean. *Divers. Distrib.* **28**, 142–159 (2022).
31. L. G. Torres, *et al.*, Demography and ecology of southern right whales *Eubalaena australis* wintering at sub-Antarctic Campbell Island, New Zealand. *Polar Biol.* **40**, 95–106 (2017).
32. P. Costa, R. Praderi, M. Piedra, P. Franco-Fraguas, Sightings of southern right whales, Eubalaena australis, off Uruguay. *Lat. Am. J. Aquat. Mamm.* **4**, 157–161 (2005).
33. C. M. Kemper, *et al.*, Encounter Bay, South Australia, an important aggregation and nursery area for the southern right whale, *Eubalaena australis* (Balaenidae: Cetacea). *Trans. R. Soc. South Aust.*, DOI: 10.1080/03721426.2021.2018759 (2022).
34. V. J. Rowntree, R. Payne, D. Schell, Changing patterns of habitat use by southern right whales (*Eubalaena australis*) on their nursery ground at Península Valdés, Argentina, and in their long-range movements. *J. Cetacean Res. Manag. Spec. Issue* **2**, 133–143 (2001).
35. E. L. Carroll, *et al.*, Genetic diversity and connectivity of southern right whales (*Eubalaena australis*) found in the Brazil and Chile-Peru wintering grounds and the South Georgia (Islas Georgias del Sur) feeding ground. *J. Hered.* **111**, 263–276 (2020).
36. A. N. Zerbini, *et al.*, Tracking southern right whales through the southwest Atlantic:

new insights into migratory routes and feeding grounds. Report SC/66b/BRG26 presented to the Scientific Committee of the International Whaling Commission, Cambridge, UK. Available from https:/ (2015).
37. A. N. Zerbini, *et al.*, Satellite tracking of Southern right whales (*Eubalaena australis*) from Golfo San Matías, Rio Negro Province, Argentina. *Rep. SC/67B/CMP17 to Sci. Comm. Int. Whal. Comm. Cambridge, UK. Available from https//iwc.int* (2018).
38. K. St John Glew, *et al.*, Isoscape Models of the Southern Ocean: Predicting Spatial and Temporal Variability in Carbon and Nitrogen Isotope Compositions of Particulate Organic Matter. *Global Biogeochem. Cycles* **35** (2021).
39. S. Todd, P. Ostrom, J. Lien, J. Abrajano, Use of biopsy samples of humpback whale (*Megaptera novaeangliae*) skin for stable isotope (δ13C) determination. *J. Northwest Atl. Fish. Sci.* **22**, 71–76 (1997).
40. L. O. Valenzuela, M. Sironi, V. J. Rowntree, J. Seger, Isotopic and genetic evidence for culturally inherited site fidelity to feeding grounds in southern right whales (Eubalaena australis). *Mol. Ecol.* **18**, 782–791 (2009).
41. L. O. Valenzuela, M. Sironi, V. J. Rowntree, Interannual variation in the stable isotope differences between mothers and their calves in southern right whales (*Eubalaena australis*). *Aquat. Mamm.* **36**, 138–147 (2010).
42. E. L. Carroll, *et al.*, Variation in $\delta^{13}C$ and $\delta^{15}N$ values of mothers and their calves across southern right whale nursery grounds : the effects of nutritional stress ? 1–14 (2021).
43. G. L. van den Berg, *et al.*, Decadal shift in foraging strategy of a migratory southern ocean predator. *Glob. Chang. Biol.* **27**, 1052–1067 (2021).
44. E. L. Carroll, *et al.*, Cultural traditions across a migratory network shape the genetic structure of southern right whales around Australia and New Zealand. *Sci. Rep.* **5**, 16182 (2015).